Journal of Cleaner Production 428 (2023) 139350

Contents lists available at ScienceDirect

Journal of Cleaner Production

journal homepage: www.elsevier.com/locate/jclepro

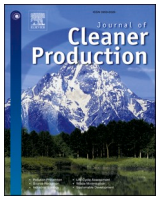

Multi-objective scheduling of a steelmaking plant integrated with renewable energy sources and energy storage systems: Balancing costs, emissions and make-span

Pengfei Su, Yue Zhou *, Jianzhong Wu

School of Engineering, Cardiff University, Cardiff, CF24 3AA, UK

ARTICLE INFO

Handling Editor: Panos Seferlis

Keywords:
Steel industry
Sustainability
Multi-objective scheduling
Uncertainties
Energy storage system
Resource task network

ABSTRACT

As an energy-intensive industry, the steel industry grapples with increasing energy costs and decarbonisation pressures. Therefore, multi-objective optimisation is widely applied in the production scheduling of the steelmaking plant. However, the optimal solution prioritising energy savings and emission reductions may lead to impractical or less economically efficient solutions, since the processing time requirement (PTR) of steel production orders in real-world production is neglected. This study fills the research gap by discussing the impact of PTR on the make-span of the steelmaking process and incorporating it into the optimisation model. Considering the variability of PTR, the solving of the multi-objective scheduling problem is transformed into the selection from Pareto solutions with different make-spans. To better leverage the temporal flexibility of the steelmaking process, a what-if-analysis-based strategy coupled with the Normal Boundary Intersection method is proposed to generate a series of evenly distributed Pareto solutions. The energy storage system is integrated to improve the time granularity of the steelmaking plant's flexibility. Our case studies demonstrate that the electricity and emission costs are reduced by 68.5%, indirect emissions are reduced by 83.5%, and the on-site renewable energy self-consumption rate increases by 12.1%. The effectiveness of the proposed method implies that it is of great relevance to the development of a cleaner steel industry in the future.

1. Introduction

Steel, as a cornerstone of modern economies and a linchpin of the energy transition, is responsible for approximately 8% of global energy demand and 7% of energy sector CO2 emissions (IEA, 2020). The imperative of reducing these emissions by at least 50% by 2050 (IEA, 2020) is challenged by the steel industry's heavy coal dependency (Sun et al., 2020), making steel industry emissions "hard-to-abate". Among commercialised steelmaking technologies, secondary steelmaking, which recycles scrap metal, promotes resource efficiency and emission reduction in the steel industry. However, its inherently electricity-intensive nature results in high electricity costs and increased grid-related indirect emissions. The steelmaking[1] process is identified for its substantial potential in offering demand-side flexibility (Zhang et al., 2017; Wang et al., 2023a), as its large electricity consumption and power demand, and well-established infrastructures for control and communication. A strategic production schedule is highly desirable for substantial electricity cost savings and to mitigate indirect emissions without significant capital investments.

Existing literature predominantly centres on single objectives, prioritising either make-span minimisation or electricity cost reduction. The objective for optimal scheduling of steel plants has traditionally been focused on minimising the make-span (Harjunkoski and Grossmann, 2001; Harjunkoski and Sand, 2008) to promote rapid production, thereby fully utilising the heavily invested facilities. In recent times, smart grid technologies and the liberalisation of the energy markets have allowed steel plants to actively participate in demand response or demand side management to optimise their electricity costs. Given the recent surge in electricity prices, minimising electricity costs has become a priority for steelmaking plants. Strategies for energy-aware scheduling have been explored with a variety of emphases, such as peak load management (Ashok, 2006; Wang et al., 2023b; Zhang et al., 2017), electricity cost reduction (Castro et al., 2009, 2013, 2019, 2020) and ancillary services provision (Ramin et al., 2018; Xu et al., 2020, 2021).

* Corresponding author.
E-mail addresses: sup2@cardiff.ac.uk (P. Su), zhouy68@cardiff.ac.uk (Y. Zhou), wuj5@cardiff.ac.uk (J. Wu).

[1] Hereby, without specific clarification, the term steelmaking referes to secondary steelmaking.

https://doi.org/10.1016/j.jclepro.2023.139350
Received 20 June 2023; Received in revised form 27 September 2023; Accepted 15 October 2023
Available online 16 October 2023

Although a significant decrease in electricity costs is evident, other objectives in production schedules, such as emission reduction and make-span minimisation, are often neglected. Multi-objective optimisations considering both cost and emission reduction are emphasised by some studies. Given the concerns regarding fossil fuel usage and its resultant greenhouse gas emissions, grid-related carbon emissions have likewise been highlighted in the literature. Zhang et al. (2014) examined the trade-off between electricity costs and grid-associated carbon emissions while not compromising production throughput under time-of-use tariffs for a flow shop. For the scheduling of a steelmaking process, current studies have mainly two limitations: 1) the existing model of the steelmaking process is not compact enough; 2) the processing time requirement (PTR) of steel production orders is overlooked.

The scheduling of the steelmaking process is often recognised as one of the most intricate industrial scheduling problems, as it is a large-scale, multistage, multiproduct batch process encompassing parallel equipment and critical production-related constraints (Harjunkoski and Grossmann, 2001). The resource-task network (RTN) serves as a proficient modelling framework, systematically illustrating intricate chemical processes. Castro et al. (2013) validate the effectiveness of the RTN model for developing a steelmaking process model, effectively capturing the key scheduling constraints of a steel plant. However, the modelling of indirect emissions is neglected in the RTN model. Thus, to be applied to the multi-objective scheduling problem, both electricity consumption and indirect emission need to be included in the RTN model.

PTR refers to the maximum completion time of the steelmaking order required by the customers. The variability of the PTR arises from order modifications, such as rush order arrival, order cancellation, and changes in due dates (either delays or advances) (Iglesias-Escudero et al., 2019; Xiong et al., 2022). In the steelmaking process, PTR is the direct factor that affects the to-be-selected make-span of the steelmaking plant, which directly impacts the temporal flexibility of the steel production process. Trevino-Martinez et al. (2022) develop an energy-carbon footprint optimisation model for a single-machine scheduling problem, generating a schedule with a singular make-span. However, only considering a singular make-span leads to some critical problems. When the PTR is shorter than the predefined make-span, the obtained solution will be impractical in real-time production, while the flexibility of the steelmaking process is not fully utilised if the PTR is way longer than the predefined make-span. Therefore, well-distributed Pareto solutions are desirable to better leverage the temporal flexibility of the steelmaking process under different PTR scenarios.

Additionally, by incorporating on-site renewable energy sources (RES) like photovoltaic (PV) and wind power, the plant's sustainability and cost-effectiveness can be significantly enhanced (Chen et al., 2022). However, the batch production mode inherent in steelmaking poses challenges for efficient renewable energy utilisation due to poor time granularity. This issue stems from a misalignment of time scales between electricity prices (e.g., a 60-min interval in the UK (NORD, 2023)), RES predictions (e.g., a 30-min interval in the UK (National Grid, 2023a)), and the batch production of secondary steelmaking (e.g., a 35–85-min continuous operating interval (Castro et al., 2013)). To tackle the poor time granularity issue, Hadera et al. (2015) proposed a continuous-time model that incorporates on-site generation and potential grid sell-back options, aiming to optimize the daily production schedules and electricity purchases of a steel plant. The proposed solution scheme benefits from the exact timing of the tasks by the continuous-time scheduling representation. However, the limitation of the continuous-time model concerning computational performance poses challenges when applied to larger instances. Another method to improve the time granularity of the batch processes' flexibility is to integrate the on-site flexible resources, e.g., energy storage system (ESS) (Li et al., 2023), into the production scheduling model. To overcome the restriction of poor granularity on offering ancillary services due to discrete power changes by switching on/off the loading units, Zhang et al. (2018) propose a method for providing ancillary services by the combination of industrial loads, which can adjust their power consumption only in large discrete steps, and an on-site ESS, which provides the more granular power adjustments. Nonetheless, considering the distinctions between steelmaking and cement production processes, further research is needed to explore how energy storage can bolster flexibility in steel production. The above literature review indicates a significant lack of studies on the coordinated optimization of ESS and industrial processes to address the limitations of poor time granularity inherent in batch production. This is particularly evident when considering the distinct challenges associated with steelmaking processes.

In this paper, we introduce a multi-objective scheduling model for a secondary steelmaking plant equipped with both RES and ESS, considering the variability in the PTR of steel production orders. Our model aims to minimise electricity costs, reduce indirect emissions, and accommodate variability in PTR, while simultaneously integrating critical steelmaking constraints to ensure operational safety and continuity. Since the PTR is an external factor that affects the make-span of the steelmaking plant, we transform the solving of the scheduling problem to the selection from Pareto solutions with different make-spans. We propose a what-if-analysis-based strategy coupled with the Normal Boundary Intersection (NBI) method to generate a series of evenly distributed Pareto solutions, which better leverage the temporal flexibility of the steelmaking process. Furthermore, to address the poor time granularity in the batch steelmaking process, we integrate the BESS into the demand response model to improve the time granularity of the steelmaking plant's flexibility. Three major contributions of this paper are summarised as follows.

1) With an extended RTN method, we present a multi-objective mixed integer linear program (MO-MILP) model that embeds critical steelmaking constraints, considering electricity cost minimisation, indirect emission reduction, and PTR variability.
2) Considering the variability in PTR, we propose a what-if-analysis-based strategy to generate a series of Pareto optimal points tailored to different make-span scenarios. To yield evenly distributed Pareto optimal points, we introduce the Normal Boundary Intersection (NBI) method to the formulation of our proposed MO-MILP model, such that the electricity cost and emission are optimised for specified make-span scenarios.
3) By integrating ESS into the demand response model, we improve the time granularity of the steelmaking plant's flexibility, which is inherently limited by the batch steelmaking process. With the improved responsiveness, the RES self-consumption of the steelmaking plant is increased, and the electricity cost and emission are reduced.

The remainder of this paper is organised as follows: Section 2 introduces the model description, while Section 3 provides the mathematical formulation of the proposed multi-objective scheduling model; Section 4 describes the what-if-analysis-based strategy coupled with the NBI method for obtaining representative optimal solutions. A case study, including the test system description and result and discussion, is provided in Section 5. Finally, Section 6 summarises the conclusion and future research.

2. Model description

2.1. Role of the proposed model in current industrial information management systems

Our multi-objective scheduling model is designed to be integrated into the current information management systems of industrial plants, as illustrated in Fig. 1. In line with industrial standards, such as the ISA-95 standard (International Society of Automation (ISA), 2020), the plant's existing information management systems consist of the enterprise resources planning (ERP) layer, the manufacturing execution system

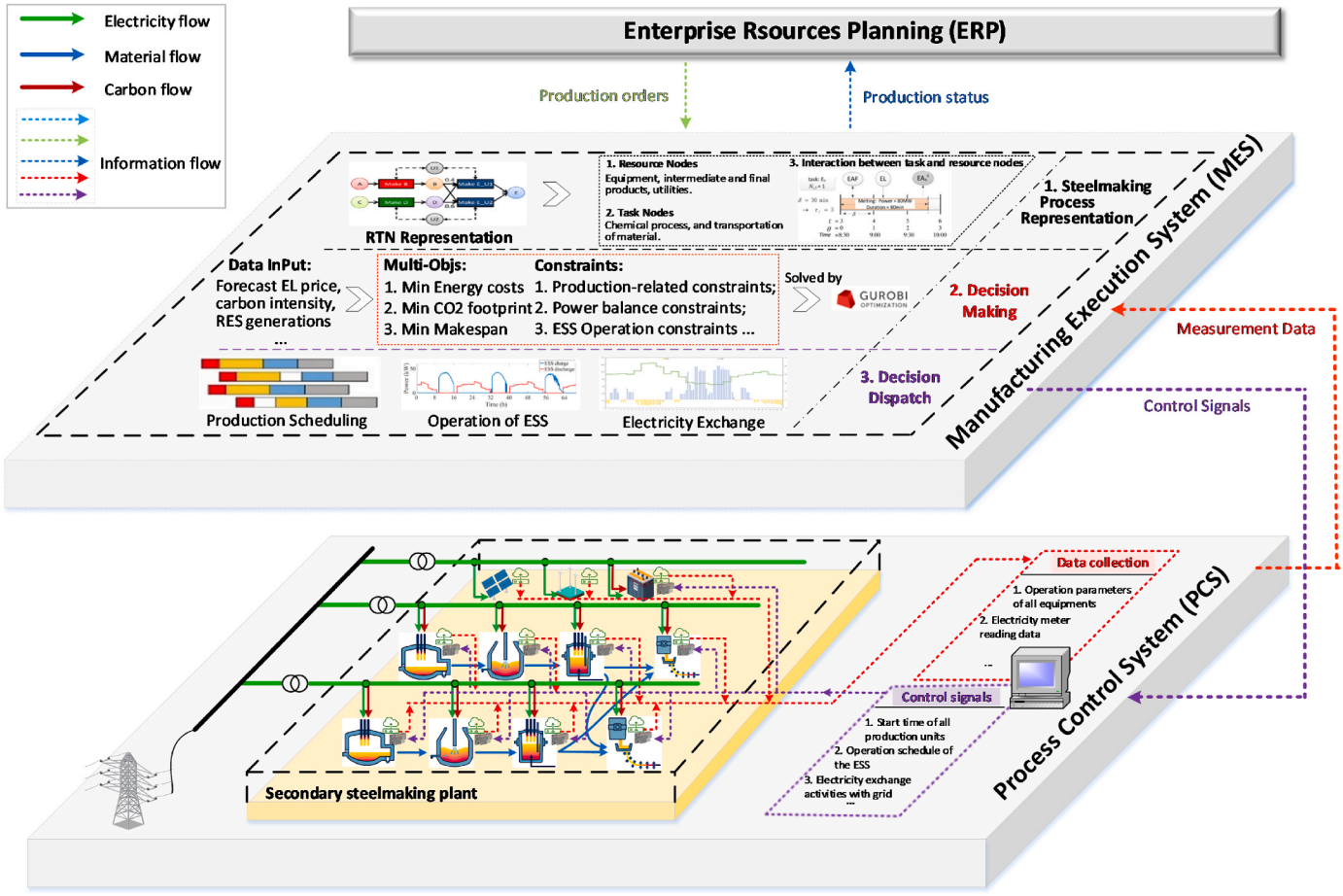

Fig. 1. Integration of the multi-objective scheduling model into the industrial information management system.

(MES) layer, and the process control system (PCS) layer (Harjunkoski et al., 2014).

From top to bottom, the ERP layer manages plant resources and operations, including inventory, procurement, sales, and finance. It generates production orders based on customer demands, which are then executed in the MES and PCS layer. The ERP layer also receives information from the MES layer to inform enterprise-level decision-making, such as production status and inventory levels.

The MES layer acts as the intermediary between the ERP and the PCS layers. Within the MES layer, our core decision-making process occurs, optimising a multi-objective schedule through a structured workflow that encompasses steelmaking process representation, decision-making, and decision dispatch stages. Once the optimal results are determined, they are converted into control signals within the MES layer and dispatched to the PCS layer. These control signals dictate the start time for all production units, the operation schedule of the ESS and electricity exchange with the grid, effectively coordinating the production processes and energy management.

The PCS layer is responsible for monitoring and controlling the actual production processes. It collects real-time data from sensors and equipment, such as electricity meter reading data, and operation parameters of all equipment (e.g., temperature and pressure inside the steelmaking units, power flow, state of charge of the ESS, etc.), to ensure that the production processes are running smoothly and within specified parameters. The PCS layer also receives control signals from the MES layer to adjust the operation of production units as needed.

2.2. Characteristics of the steelmaking process

The steelmaking process, as illustrated in Fig. 2, consists of four stages: electric arc furnace (EAF), argon oxygen decarburisation (AOD), ladle furnace (LF), and continuous casting (CC). In the EAF stage, the raw material is melted into molten metal. The AOD stage is responsible for purifying the molten metal and reducing its carbon content. The LF stage further refines the metal and transfers it to the CC stage, where it is cast into various shapes, such as slabs. To meet customer requirements, the final products have different characteristics, including grade, width, and thickness (Zhang et al., 2017). Generally, the plant involves parallel equipment and various critical production-related constraints (Harjunkoski and Sand, 2008). Each stage of the steel manufacturing process has

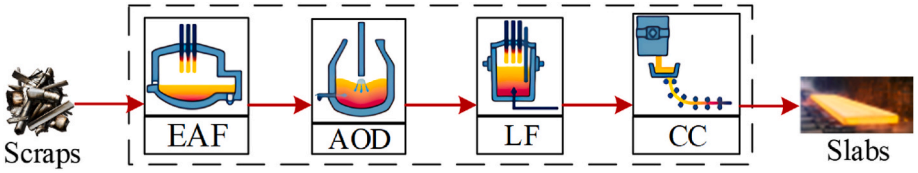

Fig. 2. A typical secondary steelmaking process.

specific energy requirements and consumption patterns. The batch production mode, characterised by the processing of heat, which refers to a batch of molten metal, often leads to poor time granularity, thereby diminishing demand flexibility.

The main difficulty of the scheduling of the steelmaking process primarily stems from the large number of discrete variables in the model (Zhang et al., 2017). To model and optimise the scheduling of steelmaking plants, the RTN is widely used because of the reduced computational complexity and the negligible differences in the final solution compared to the solutions of more rigorous models, which take a significantly longer time to run. The RTN formulations of the steelmaking critical constraints are detailed in prior studies (Castro et al., 2013; Zhang et al., 2017). Our study extends RTN formulations by including grid-related indirect emissions and then incorporates them into our multi-objective scheduling model.

2.3. RTN-based representation of the steelmaking process

The RTN, as illustrated in Fig. 3, serves as an effective tool for representing the steelmaking process through the delineation of "resources", "tasks", and "networks". The "resources" encompass various production entities, such as equipment units, intermediate and final products, as well as utilities like electricity consumption (EC) and carbon emissions (CE). The resource set $\mathbb{R}$ is depicted in Eq. (1).

$$\begin{aligned}\mathbb{R} = &\{EAFs, AODs, LFs, CC_1, CC_2\}\\ \cup&\left\{EA_h^s, EA_h^d, AL_h^s, AL_h^d, LC_h^s, LC_h^d, H_h \middle| h \in \mathbb{H}\right\}\\ &\cup\{EC, CE\}\end{aligned} \tag{1}$$

where $\mathbb{H}$ is the set of heats to produce; $\{EAFs, AODs, LFs, CC_1, CC_2\}$ represents equipment units in the four stages; $\{EA_h^s, EA_h^d, AL_h^s, AL_h^d, LC_h^s, LC_h^d\}$ indicates the set of intermediate products distinguished by their locations as either the starting point or destination of a corresponding transfer, which is marked with superscripts s or d, respectively; H_h represents the set of final products; and $\{EC, CE\}$ represents the set of utilities like EC and CE.

The tasks in the proposed model represent the operation activities performed during the steelmaking process. There are seven types of tasks: the first three operational tasks $\{E_h, A_h, L_h | h \in \mathbb{H}\}$ corresponding to each of the first three stages, the casting tasks $C_{g,u}$ for the CC stage executed by the caster unit u for each casting campaign group g, and the three transfer tasks $\{EA_h, AL_h, LC_h | h \in \mathbb{H}\}$ between these stages. The set of tasks is denoted by $\mathbb{N}$, as given in Eq. (2).

$$\begin{aligned}\mathbb{N} = &\{E_h, A_h, L_h, EA_h, AL_h, LC_h | h \in \mathbb{H}\}\\ &\cup\left\{C_{g,u} \middle| g \in \mathbb{G}, u \in \mathbb{U}\right\}\end{aligned} \tag{2}$$

where $\mathbb{G} = \{G_1, G_2, \cdots, G_g\}$ and $\mathbb{U} = \{CC_1, CC_2\}$ are the sets of casting campaign groups and available casters, respectively.

The network component of the RTN framework captures the relationships and dynamics between tasks and resources. The network flowchart in Fig. 3 indicates the relationships between each task and its related resources. Processing tasks exhibit continuous interaction with EC and CE resources, while their interaction with other resources is discrete. Continuous interaction implies consistent consumption or generation of resources throughout a task's duration. Conversely, discrete interaction signifies interactions that occur at specific, distinct time points during the task.

The discrete-time representation is utilised in the RTN model (Pantelides, 1994). As illustrated in Fig. 4, the discrete-time formulation corresponds to a uniform time grid, consisting of T slots with a specific length δ (min) spanning 24 h. The time grid starts from $t = 1$ and ends $t = \mathrm{T}$. The processing time for all tasks is rounded to a multiple of δ. Specifically, the duration of the task n, measured in the number of time slots, is calculated by Eq. (3).

$$\tau_n = \lceil d_n / \delta \rceil \tag{3}$$

where d_n is the processing duration of the task n measured in minutes; $\lceil . \rceil$ is the rounding up operator.

The dynamics between tasks and resources are associated with an interaction parameter $\mu_{r,i,\theta}$ for each task $i \in \mathbb{N}$, representing the amount of resource r consumed or generated by the task i at a specific relative time slot $\theta - th$ after the start of the task i with the value set $\{-1, 0, 1\}$.

The interaction parameters for the decarburisation task processed in the AOD unit with its interactive resources are illustrated in Fig. 5. The processing duration of the decarburisation task is assumed to be 80 min, and the slot length δ is assumed to be 30 min. Hence, the duration of the decarburisation task in the number of time slots can be calculated by Eq. (3), and the task spans three time slots. Note that there are three different references for time: t is the index for the uniform time grid; θ is

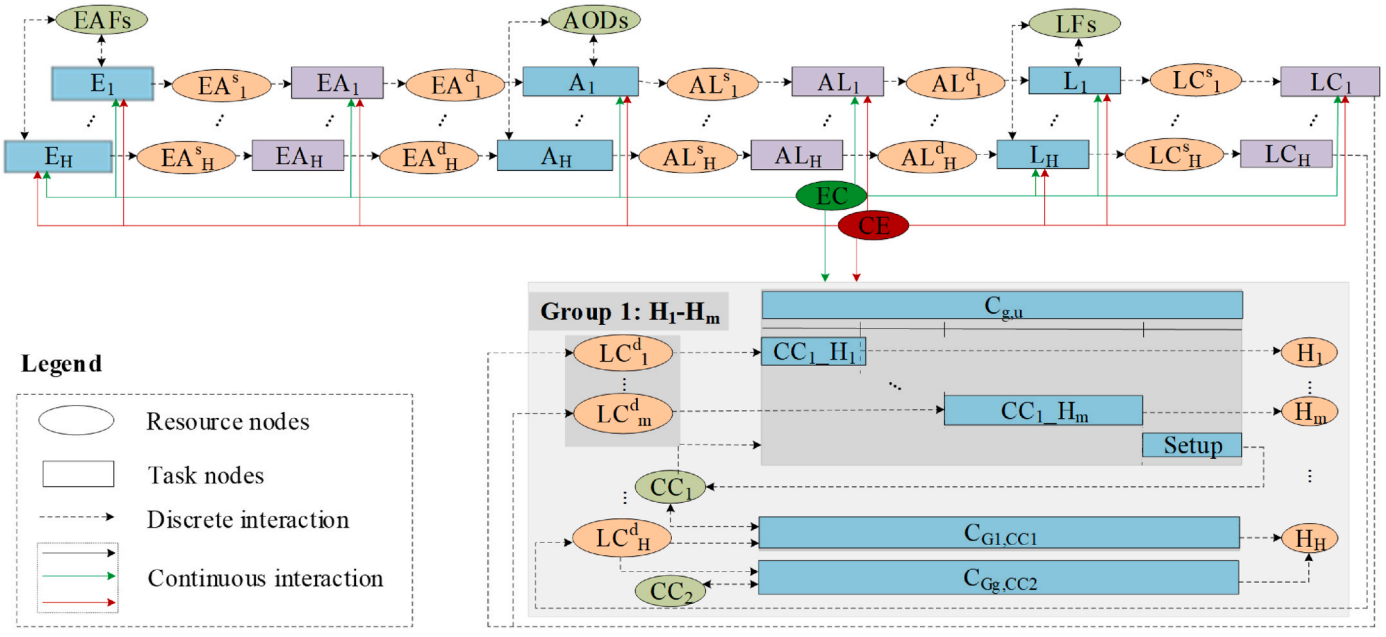

Fig. 3. Representation of the secondary steelmaking process using resource-task-network framework.

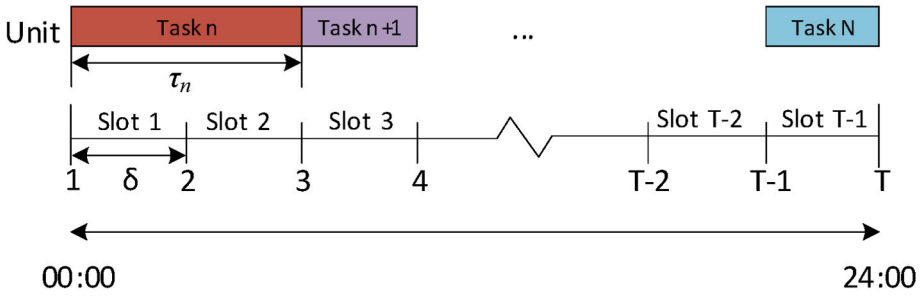

Fig. 4. Discrete-time representation of the RTN model with a uniform time grid.

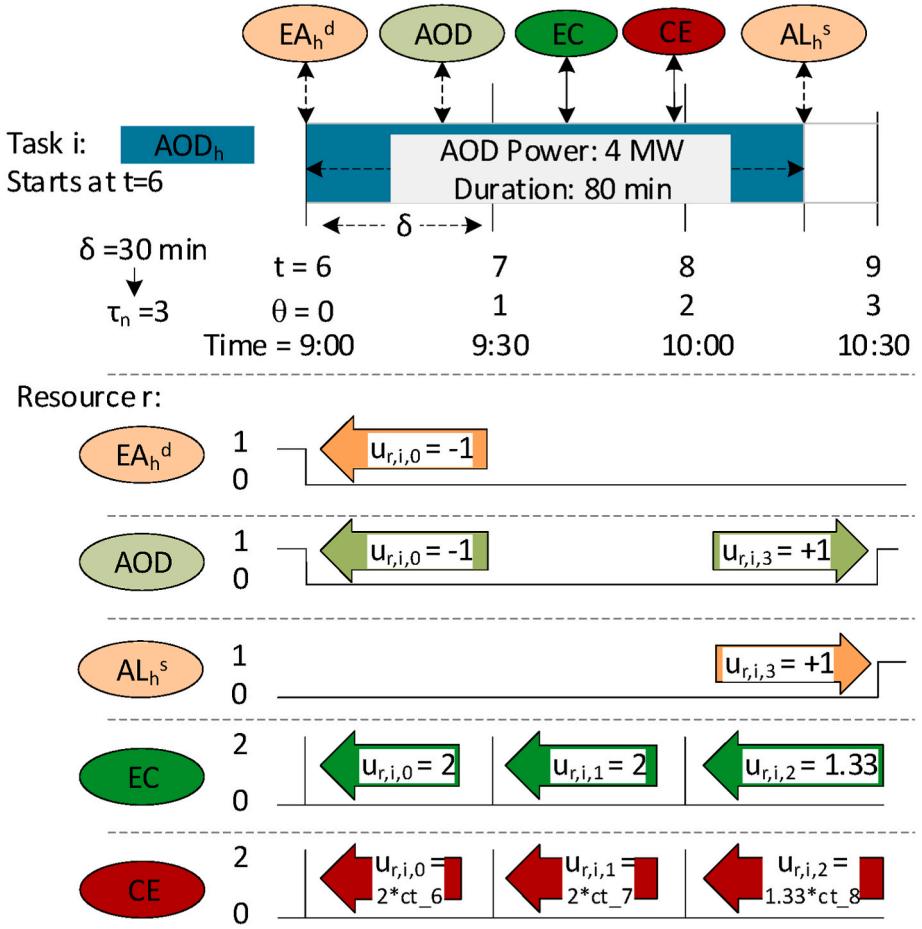

Fig. 5. Illustration of interaction parameters for a decarburisation task.

the relative time index related to the start of the task *i*, *Time* represents the actual hour of the day. The discrete-time formulation assumes that the task can only start at the beginning of the time slot but end anywhere within the time slot (Pantelides, 1994). This rounding error caused by the discrete-time formulation might underestimate the potential flexibility gained from scheduling, which, however, can be alleviated by using a finer time grid while increasing the computational complexity (Zhang et al., 2017).

In Fig. 5, the decarburisation task AOD_h of heat h interacts with resources $EA_h{}^d$, AOD, $AL_h{}^s$, EC and CE. We assume that the decarburisation task AOD_h starts at $t = 6$, intermediate product resource $EA_h{}^d$ is then reduced by one as the task consumes the intermediate product generated by the previous stage; meanwhile, the equipment resource AOD is also reduced by one as the operation unit is occupied at this time. After the decarburisation process is done, AOD is increased by one as the decarburisation equipment unit is freed up; meanwhile, the intermediate product resource $AL_h{}^s$ is increased by one to promote the execution of the following transfer. Throughout the process, EC is continuously consumed, while CE is continuously generated. This CE is a product of the EC and the region carbon intensity ct_t at time slot t. Note that the electricity consumption and carbon emissions for the final time slot are less than the previous two slots because the task finishes early before the end of that slot (Zhang et al., 2017).

3. Mathematical formulation

With the extended RTN method, we present a MO-MILP model of the multi-objective scheduling of a steelmaking plant. This model embeds critical steelmaking constraints, ESS operation constraints and power balance constraints, considering electricity cost reduction, indirect emission reduction, and PTR variability.

3.1. Constraints

3.1.1. Critical steelmaking-related constraints

3.1.1.1. Resource balance constraints. The resource balance constraints manage the interaction between each resource and its relevant tasks over the time grid by Eq. (4).

$$R_{r,t} = R_{r,t-1} + \sum_{i}\sum_{\theta=0}^{\tau_i} \mu_{r,i,\theta} I_{i,t-\theta} \forall t \in \mathbb{T}, r \in \mathbb{R}_{\neg\{EC,CE\}} \tag{4}$$

where $R_{r,t}$ denotes the value of resource r at the time slot t, which is computed as its preceding value $R_{r,t-1}$ adjusted by the quantity produced or consumed by all tasks; $\mu_{r,i,\theta}$ represents the interaction quantity between resource r and task i at the $\theta - th$ time slot since the start of the task i. Here, $\mathbb{T}$ is the set of all time slots, while $\mathbb{R}_{\neg\{EC,CE\}}$ is the set of all resources excluding resources of EC and CE.

The resources in Eq. (4) purposely exclude EC and CE as they are calculated individually for each time slot, thereby eliminating any propagation effects from the preceding time slot. The resource balance constraints for resources EC and CE are determined by Eq. (5).

$$\Pi_{r,t} = \sum_{i}\sum_{\theta=0}^{\tau_i} \mu_{r,i,\theta} I_{i,t-\theta} \quad \forall t \in \mathbb{T}, r \in \mathbb{R}_{\{EC,CE\}} \tag{5}$$

where $\Pi_{r,t}$ denotes the value of resources r (e.g. EC and CE) at the time slot t.

3.1.1.2. Task execution constraints. To ensure immediate execution of transfer tasks, intermediate products produced by its preceding processing tasks are set to 0, as defined by Eq. (6). Additionally, Eq. (7) ensures that final products must be ready for delivery by the final time slot by making the resource value of the final product equal to 1. For the first three stages, task execution constraints, as detailed in Eq. (8), stipulate that each heat is processed exactly once within the scheduling horizon. Transfer of all intermediate products occurs only once as defined by Eq. (9). Finally, for each group g in the final stage, Eq. (10) mandates that each group undergoes processing exactly once by any unit u from the available casters, validated by ensuring that the sum of all processing task variables over the time horizon and all potential casters equal 1.

$$R_{EA_h^s,t} = R_{AL_h^s,t} = R_{LC_h^s,t} = 0 \quad \forall h \in \mathbb{H} \tag{6}$$

$$R_{H_h,|\mathbb{T}|} = 1 \quad \forall h \in \mathbb{H} \tag{7}$$

$$\sum_{t\in\mathbb{T}} I_{i_{EAF_h},t} = \sum_{t\in\mathbb{T}} I_{i_{AOD_h},t} = \sum_{t\in\mathbb{T}} I_{i_{LF_h},t} = 1 \quad \forall h \in \mathbb{H} \tag{8}$$

$$\sum_{t\in\mathbb{T}} I_{i_{EA_h},t} = \sum_{t\in\mathbb{T}} I_{i_{AL_h},t} = \sum_{t\in\mathbb{T}} I_{i_{LC_h},t} = 1 \quad \forall h \in \mathbb{H} \tag{9}$$

$$\sum_{u\in\mathbb{U}}\sum_{t\in\mathbb{T}} I_{i_{C_{g,u}},t} = 1 \quad \forall g \in \mathbb{G}, u \in \mathbb{U} \tag{10}$$

3.1.1.3. Transfer time constraints. To mitigate potential product quality degradation caused by adverse cooling effects, transfer time constraints are also considered. These constraints apply particularly to intermediate products (e.g., w_{EA}, w_{AL} and w_{LC}), as excessive cooling might necessitate costly reheating. Transfer time is considered independent of specific heats and equipment units, while a maximum allowable transfer time (e.g., W_{EA}, W_{AL} and W_{LC}) is defined to preclude cooling effects. Accordingly, the combined transfer and waiting time for intermediate products are constrained to an upper bound, as enforced by Eq. (11).

$$\begin{cases} \delta\sum_{t\in\mathbb{T}} R_{EA_h^d,t} + w_{EA} \le W_{EA} & \forall h \in \mathbb{H} \\ \delta\sum_{t\in\mathbb{T}} R_{AL_h^d,t} + w_{AL} \le W_{AL} & \forall h \in \mathbb{H} \\ \delta\sum_{t\in\mathbb{T}} R_{LC_h^d,t} + w_{LC} \le W_{LC} & \forall h \in \mathbb{H} \end{cases} \tag{11}$$

where $\sum_{t\in\mathbb{T}} R_{EA_h^d,t}$, $\sum_{t\in\mathbb{T}} R_{AL_h^d,t}$ and $\sum_{t\in\mathbb{T}} R_{LC_h^d,t}$ denote the total time slots during which intermediate products wait before proceeding to the next processing stage while δ symbolising the length of each time slot.

3.1.2. ESS operation constraints

Battery energy storage systems (BESS) are considered, and the related operation constraints are presented below.

3.1.2.1. State dynamics constraints. These constraints, detailed in Eq. (12), relate to the energy stored in the BESS and the charging/discharging power across two consecutive time slots, considering both charging and discharging efficiencies.

$$E_{B,t} = \begin{cases} E_{B,t-1} - \dfrac{P_{B,t}\cdot\Delta t}{\eta^{Dis.}}, & if \quad P_{B,t} > 0 \\ E_{B,t-1} - P_{B,t}\cdot\Delta t\cdot\eta^{Ch.}, & if \quad P_{B,t} \le 0 \end{cases}, \quad t \in \mathbb{T} \tag{12}$$

where $E_{B,t}$ represents the energy stored in the BESS at the time t, Δt is the time interval, $\eta^{Ch.}$ and $\eta^{Dis.}$ are the charging and discharging efficiencies of the BESS. $P_{B,t}$ denotes the power of the BESS; when $P_{B,t} > 0$, it indicates discharging, and vice versa.

3.1.2.2. State of charge constraints. The state of charge (SoC) is defined as Eq. (13). To prevent the BESS from being over-charged or over-discharged, the SoC limit constraints are defined as Eq. (14).

$$SoC_t = \frac{E_{B,t}}{E_B^{Cap.}}, \quad t \in \mathbb{T} \tag{13}$$

$$SoC^{Min} \le SoC_t \le SoC^{Max}, \quad t \in \mathbb{T} \tag{14}$$

where $E_B^{Cap.}$ indicates the capacity of BESS; SoC^{Min} and SoC^{Max} are the lower and upper bounds of SoC, respectively.

Additionally, to ensure that the SoC at the end of the day remains the same as the SoC at the beginning of the day, the constraint is enforced as Eq. (15).

$$SoC_{|\mathbb{T}|} = SoC_1 \tag{15}$$

where $|\mathbb{T}|$ indicates the final time slot of the day.

3.1.2.3. Power capacity constraints. The power capacity limit is enforced by Eq. (16).

$$P_B^{Min} \le P_{B,t} \le P_B^{Max}, \quad t \in \mathbb{T} \tag{16}$$

where P_B^{Min} and P_B^{Max} are the lower and upper bounds of the BESS power capacity, respectively.

3.1.3. Power balance constraints

Power balance constraints ensure the balance of the electricity consumed and generated, as shown in Eq. (17). Additionally, the power exchange with the utility grid is bounded, as enforced by Eq. (18).

$$P_{EL,t} = P_{U,t} + P_{B,t} + P_{PV,t} + P_{WT,t}, \quad t \in \mathbb{T} \tag{17}$$

$$P_U^{Min} \le |P_{U,t}| \le P_U^{Max}, \quad t \in \mathbb{T} \tag{18}$$

where $P_{EL,t}$ represents the electricity consumption of the steel plant at

the time slot t; $P_{U,t}$ denotes the amount of electricity purchased from the utility grid, where $P_{U,t} > 0$ represents buying electricity from the utility grid, and vice versa; $P_{PV,t}$ and $P_{WT,t}$ are electricity generated by solar panels and wind turbines, respectively; P_U^{Max} and P_U^{Min} represent the upper and lower bounds of the transmission capacity of the power line between the steel plant and the utility grid.

3.2. Multi-objective functions

3.2.1. Make-span objective

The make-span objective aims to minimise the overall production completion time *Makespan*, as defined in Eq. (19). Typically, the make-span is determined by the completion time of the last group processed in the continuous casters. However, due to the uncertainty of which group will finish last, we constrain the make-span to be greater than or equal to the completion time for all potential scenarios of group completion, as shown in Eq. (20) (Castro et al., 2013).

$$Min \quad Makespan \tag{19}$$

$$Makespan \geq \sum_{i \in N_{g,u}} \sum_{t \in \mathbb{T}} I_{i_{C_{g,u}},t}((t-1)\delta + \tau_i \delta - setup_u) \quad g \in \mathbb{G}, u \in \mathbb{U} \tag{20}$$

where $I_{i_{C_{g,u}},t}$ is the binary variable indicating whether the task $i_{C_{g,u}}$ starts at the time slot t; $i_{C_{g,u}}$ represents the casting task of casting campaign group g processed by caster unit u; τ_i represents the length (in time slots) of the task i; $setup_u$ indicates the setup duration of caster unit u.

3.2.2. Electricity and emission cost objective

3.2.2.1. Net electricity cost objective. The net electricity cost objective is calculated by subtracting the revenue from selling electricity to the grid from the electricity purchase costs overall time slots. This objective function is represented in Eq. (21).

$$Min \quad C_{EL} = \sum_{t \in \mathbb{T}} \left(\frac{P_t^{G \to I}}{\eta^T} \cdot \lambda_t^{Buy} - P_t^{I \to G} \cdot \eta^T \cdot \lambda_t^{Sell} \right) \tag{21}$$

$$\begin{cases} P_t^{G \to I} = P_{U,t}, & if \quad P_{U,t} > 0 \\ P_t^{I \to G} = -P_{U,t}, & if \quad P_{U,t} \leq 0 \end{cases} \quad t \in \mathbb{T} \tag{22}$$

where C_{EL} represents net electricity costs; $P_t^{G \to I}$ indicates power flowing from the grid to the steel plant at time slot t; $P_t^{I \to G}$ refers to power flowing from the steel plant to the grid; η^T is the efficiency of the transformer between the plant and the grid; λ_t^{Buy} is the electricity purchase price; λ_t^{Sell} refers to the electricity price when exporting electricity to the grid.

3.2.2.2. Indirect emission cost objective. Grid-related indirect emissions are monetised by multiplying the number of emissions by the carbon tax, as shown in Eq. (23).

$$Min \quad C_{EM} = p_{ct} * \sum_{t \in \mathbb{T}} \frac{P_t^{G \to I}}{\eta^T} \cdot CI_t^{CO2} \tag{23}$$

where C_{EM} indicates emission costs; p_{ct} represents the carbon tax; CI_t^{CO2} refers to the forecasted carbon intensity of the local power grid at time slot t.

Therefore, the electricity and emission cost objective function C_{TC} encompasses both the net electricity costs and indirect emissions costs, as formulated in Eq. (24).

$$Min \quad C_{TC} = C_{EL} + C_{EM} \tag{24}$$

4. What-if-analysis-based strategy for representative optimal solutions

In this section, we propose a what-if-analysis-based strategy coupled with the NBI method to our proposed MO-MILP formulation for generating a series of well-distributed optimal solutions, better leveraging the temporal flexibility of the steelmaking process.

4.1. What-if-analysis-based strategy in the steelmaking scheduling

In the steelmaking process, PTR is the direct factor that affects the to-be-selected make-span of the steelmaking plant, which directly impacts the temporal flexibility of the steel production process. Meanwhile, PTR is an external factor that is usually determined by the customers, and it serves as a prerequisite parameter of the optimal scheduling problem of the steelmaking plant. Thus, in our study, we consider the variability of PTR using "what-if" analysis, while the variability of other parameters is considered within the optimisation problem.

We incorporate a "what-if" analysis into the MO-MILP problem, treating make-span minimisation as one of the objectives. Then, we solve the multi-objective scheduling optimisation problem to generate the Pareto solutions corresponding to different make-span scenarios. Upon addressing the multi-objective optimisation, we can identify the boundary of make-span: its minimal and maximal values. Then, the impact of different make-spans within the boundary on the other objective values of the multi-objective model along the Pareto front is analysed, aiming to pinpoint the minimum cost strategy under each make-span scenario. Considering the direct relationship between PTR and make-span, the above analysing process is equivalent to the "what-if" analysis of the variability of PTR.

For the proposed multi-objective scheduling problem, we assume that minimising make-span objective is $f_1(\chi)$ and minimising electricity and emission cost objective is $f_2(\chi)$, as abstractly represented in Eq. (25), whose feasible region is Ω defined by a set of inequality constraints $g(\chi) \leq 0$ and equality constraints $h(\chi) = 0$.

$$\begin{aligned} &Min \quad \{f_1(\chi), f_2(\chi)\} \quad \chi \in \Omega \\ &s.t. \quad g(\chi) \leq 0; \quad h(\chi) = 0 \end{aligned} \tag{25}$$

By employing what-if analysis, we anticipate generating a series of n solutions $f_1(\chi_1), f_1(\chi_2), \cdots, f_1(\chi_n)$ adaptable to various PTR scenarios. where $\chi_1, \chi_2, \cdots, \chi_n$ represents solutions on the Pareto front in multi-objective optimisation, and each corresponding $f_2(\chi_1), f_2(\chi_2), \cdots, f_2(\chi_n)$ for $\chi_1, \chi_2, \cdots, \chi_n$ is ensured the optimal cost for the specific PTR scenario.

To ensure comprehensive coverage across possible PTR scenarios, it's pivotal to get a uniform distribution of the Pareto optimal solutions to enhance the adaptability and responsiveness of the model when navigating variability in PTR.

4.2. Pareto optimal solutions attainment using the NBI method

The NBI method was introduced by Das and Dennis (1998) to identify uniformly distributed Pareto-optimal solutions for nonlinear multi-objective optimisation problems. Unlike the weighted-sum (WS) approach, which struggles to achieve a uniform distribution of Pareto-optimal solutions even with evenly spread weight vectors (Shukla and Deb, 2007), the NBI method employs a scalarisation scheme that ensures that a consistent spread in parameters results in a nearly uniform distribution of points on the efficient frontier. Additionally, this method remains unaffected by the varying scales of different objective functions. The scalarisation scheme is briefly described in three steps: 1) Objective function normalisation; 2) Generation of evenly distributed points on the Utopia line; and 3) Pareto front attainment.

4.2.1. Objective function normalization

Considering the disparities in dimensions and magnitudes between

the objectives of minimising make-span and total costs, it is necessary to normalise each objective function, as indicated in Eq. (26).

$$\overline{f_i}(\chi) = \frac{f_i(\chi) - f_i(\chi_i^*)}{f_i(\chi_j^*) - f_i(\chi_i^*)} \quad i,j \in \{1,2\}, i \neq j \tag{26}$$

$$f_i(\chi_i^*) = Min \quad f_i(\chi) \tag{27}$$

where $f_1(\chi_1^*)$ and $f_2(\chi_2^*)$ represent the minimisation values obtained by individually optimizing $f_1(\chi)$ and $f_2(\chi)$ in Eq. (27); $f_2(\chi_1^*)$ and $f_1(\chi_2^*)$ indicates the values of the other objective functions at χ_1^* and χ_2^*; $\overline{f_i}(\chi)$ represents the normalised value of the objective function.

4.2.2. Well-distributed points generation

As illustrated for a bi-objective case in Fig. 6, the line connecting the point $A(f_1^*(\chi_1^*), f_2(\chi_1^*))$ and $B(f_1(\chi_2^*), f_2^*(\chi_2^*))$ is referred to as the Utopia line. The line AB is divided equally to get m_k evenly distributed points. Any point P_k on this line is expressed as Eq. (28) according to the NBI method.

$$\overline{\boldsymbol{\Phi}}\boldsymbol{\beta} = \begin{bmatrix} \overline{f_1}(\chi_1^*) & \overline{f_1}(\chi_2^*) \\ \overline{f_2}(\chi_1^*) & \overline{f_2}(\chi_2^*) \end{bmatrix} \begin{bmatrix} \beta_1 \\ \beta_2 \end{bmatrix} \tag{28}$$

where $\overline{\boldsymbol{\Phi}}$ indicates the normalised payoff matrix defined in Eq. (29) considering Eq. (26); $\boldsymbol{\beta} = [\beta_1, \beta_2]^T$ is the parameterised vector corresponding to different points on the Utopia line and satisfies constraints $\beta_1 + \beta_2 = 1, \quad \beta_{1,2} \in [0,1]$.

$$\overline{\boldsymbol{\Phi}} = \begin{bmatrix} \overline{f_1}(\chi_1^*) & \overline{f_1}(\chi_2^*) \\ \overline{f_2}(\chi_1^*) & \overline{f_2}(\chi_2^*) \end{bmatrix} = \begin{bmatrix} 0 & 1 \\ 1 & 0 \end{bmatrix} \tag{29}$$

4.2.3. Pareto front attainment

A point Q_k corresponding to P_k can be expressed as Eq. (30):

$$\boldsymbol{Q_k} = \overline{\boldsymbol{\Phi}}\boldsymbol{\beta} + D_k\boldsymbol{n} \tag{30}$$

so that $\overrightarrow{P_kQ_k}$ is a vector that is perpendicular to the Utopia line, where $\boldsymbol{n} = [n_1 \quad n_2]^T = [-1 \quad -1]^T$ is the normal unit vector to the Utopia line, starting from the point P_k and D_k indicates the distance between the points Q_k and P_k. Eq. (30) can be equivalently expanded as Eq. (31) considering Eq. (28) and Eq. (29) (Roman and Rosehart, 2006):

$$\boldsymbol{Q_k} = \begin{bmatrix} \overline{f_1}(\chi_k) \\ \overline{f_2}(\chi_k) \end{bmatrix} = \begin{bmatrix} \overline{f_1}(\chi_1^*) & \overline{f_1}(\chi_2^*) \\ \overline{f_2}(\chi_1^*) & \overline{f_2}(\chi_2^*) \end{bmatrix} \begin{bmatrix} \beta_1 \\ \beta_2 \end{bmatrix} + D_k \begin{bmatrix} n_1 \\ n_2 \end{bmatrix} = \begin{bmatrix} \beta_2 - D_k \\ \beta_2 - D_k \end{bmatrix} \tag{31}$$

where, $\overrightarrow{P_kQ_k}$ is extended (by increasing D_k gradually from zero) to intersect the Pareto front at the point Q_k, so that a Pareto optimal solution (Q_k) corresponding to P_k can be obtained. This can be obtained by solving the optimization problem below:

$$Obj: \quad Max \quad D_k \tag{32}$$

$$s.t. \begin{cases} \overline{f_1}(\chi_k) = \beta_2 - D_k \\ \overline{f_2}(\chi_k) = \beta_1 - D_k \\ \beta_1 + \beta_2 = 1, \beta_{1,2} \in [0,1] \\ Constraints\ (4) - (18), (20), (22) \end{cases} \tag{33}$$

where Q_k can be calculated for each P_k obtained in Section 4.2.2, so that a total number of m_k evenly distributed points can be obtained on the Pareto front.

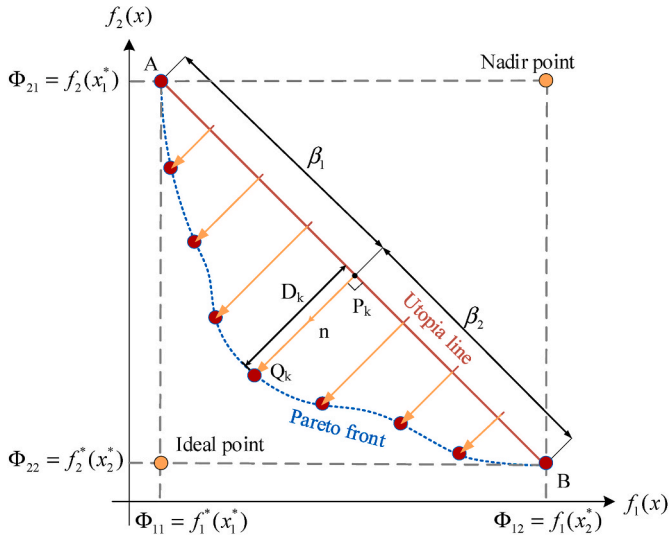

Fig. 6. The scheme of the NBI method for a bi-objective problem.

5. Case study

In this paper, a test system of a secondary steel plant in South Wales, UK, is used for the case study, focusing on a daily scheduling problem. The description of the test system and associated cases are detailed below.

5.1. Test system description

Fig. 7 shows the electricity flow within the secondary steelmaking plant. Parameters corresponding to the steelmaking plant are drawn from (Castro et al., 2013). The layout of steelmaking equipment is structured in four stages, each with two parallel machines: two EAFs, two AODs, two LFs and two CCs. The first three stages feature identical equipment units, while the fourth varies due to different setup times. Notably, nominal power consumption and processing time remain unaffected by heat specifics, as shown in Table 1 and Table 2, respectively. The setup times for the fourth-stage CCs are detailed in Table 3. Transfer times, encompassing both minimum and maximum intervals, are shown in Table 4. The complexity of the proposed model is intrinsically tied to the number of heats produced. In this case, we considered 12 heats to be produced within one day,. Each heat is affiliated with a distinct casting group, as detailed in Table 5.

Locally, the plant is equipped with a 5 MW/20 MWh Li-ion BESS, a 10 MW wind power system and a 10 MW PV system. The BESS model parameters are outlined in Table 6 (Ju et al., 2018), and per unit power outputs for RES generation are available in an online database (Pfenninger and Staffell, 2016), which are depicted in Fig. 9.

The time-varying electricity prices, presented in Fig. 8, are based on a profile of NORD POOL UK wholesale electricity prices (NORD, 2023), while the corresponding regional carbon intensity profile for the same day, illustrated in Fig. 9, is sourced from the carbon intensity API provided by the National Grid ESO (National Grid, 2023b). The carbon tax and the electricity price for export to the grid are set as £60/tCO2 and £20/MWh, respectively.

The scheduling horizon spanned a 24-h production cycle, commencing from noon of the preceding day to noon of the subsequent day, divided into 96-time slots with each being 15 min. The test run is performed in Python with Gurobi Solver on a desktop powered by an Intel Core i7 processor and 16 GB RAM.

5.2. Result and discussion

5.2.1. Performance in enhancing cost-efficiency and clean production

Three operating modes are studied to demonstrate the effectiveness

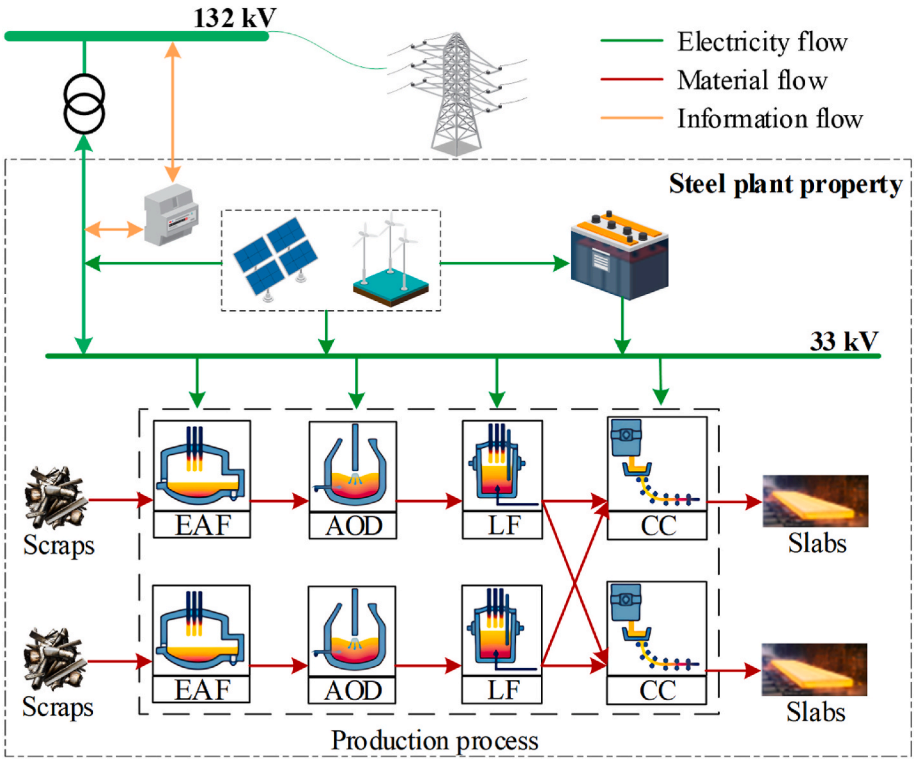

Fig. 7. The electricity flow within the secondary steel plant.

Table 1
Nominal power consumption [MW].

Unit	EAF_1	EAF_2	AOD_1	AOD_2
Power	85	85	2	2
Unit	LF_1	LF_2	CC_1	CC_2
Power	2	2	7	7

Table 2
Processing time [min].

Unit/Heat	1–4	5–6	7–8	9–12
EAF_1	80	85	85	90
EAF_2	80	85	85	90
AOD_1	75	80	80	95
AOD_2	75	80	80	95
LF_1	35	45	20	45
LF_2	35	45	20	45
CC_1	50	60	55	60
CC_2	50	60	55	60

Table 3
Setup time [min].

Unit	CC_1	CC_2
Setup time	70	50

Table 4
Transfer time [min].

Stage	EAF-AOD	AOD-LF	LF-CC
Min transfer time	10	4	10
Max transfer time	240	240	120

Table 5
Steel heat/group correspondence.

Group	G_1	G_2	G_3
Heat	1–4	5–8	9–12

Table 6
Parameters of the BESS model.

Energy Capacity (MWh)	Power Capacity (MW)	$\eta^{Ch./Dis.}$	SoC_{MAX}	SoC_{MIN}
20	5	0.95	90%	10%

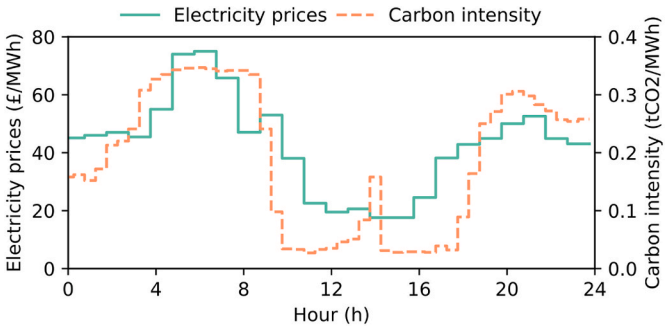

Fig. 8. Day-ahead wholesale electricity price and associated carbon intensity profiles.

of the proposed model and assess the impact of BESS incorporation:

1) SO-FixSP: Single-objective production scheduling of fixed steelmaking process with the minimum make-span but without considering demand response.

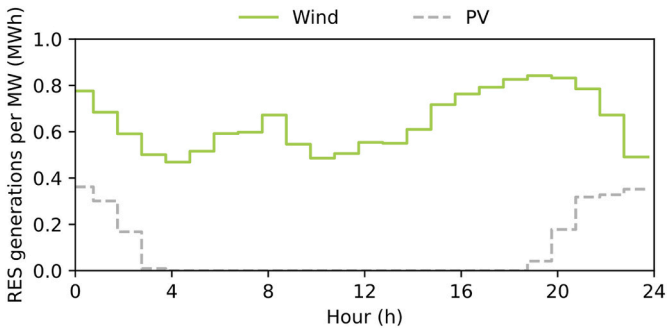

Fig. 9. RES generation per unit.

2) MO-FlexSP: Multi-objective production scheduling of flexible steelmaking process exploring the trade-off between electricity and emission costs minimisation and make-span minimisation considering demand response.
3) MO-FlexSP + BESS: Multi-objective production scheduling of flexible steelmaking process exploring the trade-off between electricity and emission costs minimisation and make-span minimisation considering coordinated demand response with BESS incorporation.

Table 7 provides a comprehensive comparison between the *SO-FixSP* case and the *MO-FlexSP + BESS* case. This comparison is made under the conditions of a £60/ton carbon tax, focusing on several performance metrics, including electricity and emission costs, indirect emissions, and RES self-consumption rate. Compared with the *SO-FixSP* case, the *MO-FlexSP + BESS* case provides a series of optimal solutions corresponding to make-spans ranging from 785 min to 1430 min. For any make-span within this range, our proposed method provides a solution with improved performance. When the make-span reaches 1430 min, the steelmaking plant achieves the best performance improvement, including a 68.5% reduction in electricity and emission costs, an 83.5% decrease in indirect emissions, and a 12.1% increase in the RES self-consumption rate.

Furthermore, to showcase the performance of the integration of BESS into the flexible steelmaking scheduling, as illustrated in Fig. 10, the integration of BESS in the *MO-FlexSP + BESS* case brings a downward shift of the Pareto front, indicating the lower total costs for all Pareto solutions due to the improvement of time granularity of steelmaking plant's flexibility. A further 4.3% decrement in electricity and emission costs is achieved when the make-span is 1430 min. The primary reason for such enhancements can be attributed to the increased flexibility granularity provided by the BESS, reinforcing the premise that BESS integration is pivotal for both cost-efficiency and cleaner production in steelmaking scheduling.

Table 7
Comparisons of electricity and emission costs and RES self-consumption among the *SO-FixSP* and *MO-FlexSP + BESS* cases (carbon tax = £60/ton).

Index	Make-span/ min	Electricity and emission costs/£	Emissions/ tCO2e	RES self-consumption rate
SO-FixSP	785	81,688	339.6	45.5%
MO-FlexSP + BESS	785	80,590	335.5	46.8%
	835	73,873	301.1	48.9%
	889	67,496	261.5	51.5%
	935	60,439	220.7	53.4%
	985	53,722	178.3	55.9%
	1045	47,855	151.2	55.5%
	1103	41,818	135.3	55.3%
	1164	36,037	112.8	57.9%
	1231	30,766	87.3	60.2%
	1312	26,684	61.8	56.8%
	1430	25,746	56.1	57.6%

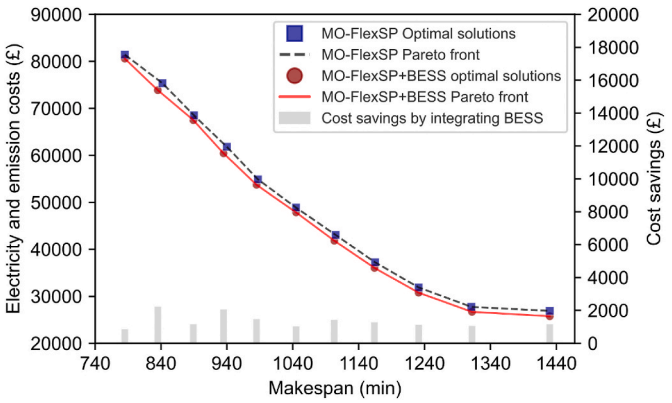

Fig. 10. Comparison of optimal solutions of the MO-FlexSP case and the MO-FlexSP + BESS case.

5.2.2. Performance in handling variability in processing time requirements

To show the even distributions of solutions obtained by the NBI method, we compare the NBI method and the weighted sum (WS) method on the distributions of the obtaining optimal solutions of different numbers. As illustrated in Fig. 11, the solutions obtained by the WS method reveal an uneven distribution that predominantly centres around a narrow range of make-span values. There is a deficiency of suitable solutions to meet the PTR within the range of 785 –1320 min. For example, when the PTR is within 1300 min, the steelmaking plant is forced to select the solution corresponding to a make-span of 785 min, satisfying part of the temporal flexibility. On the contrary, our proposed method could provide a series of evenly distributed Pareto solutions, allowing the steelmaking plant to select the solution corresponding to a make-span of 1300 min, which brings £50,923 total cost savings. Similarly, for make-spans ranging from 785 to 1320 min, the proposed method always provides an optimal solution that better leverages the temporal flexibility.

By increasing the number of Pareto points on the Pareto front, we can yield solutions with finer make-span resolution. As shown in Fig. 12, with 21 solutions, the proposed method allows the steelmaking plant to select the solution corresponding to a make-span of 1265 min, which brings a further £2579 total cost savings than the case with 11 solutions. In summary, Pareto solutions obtained by the NBI method provide a comprehensive evenly distributed representation of the trade-off between electricity and emission costs versus make-span, with a tangible decrease in costs from £81,444 to £26,899 as the make-span extends from 785 to 1430 min.

In general, the evenly distributed optimal solutions with better granularity in make-span are used in the proposed what-if-analysis-

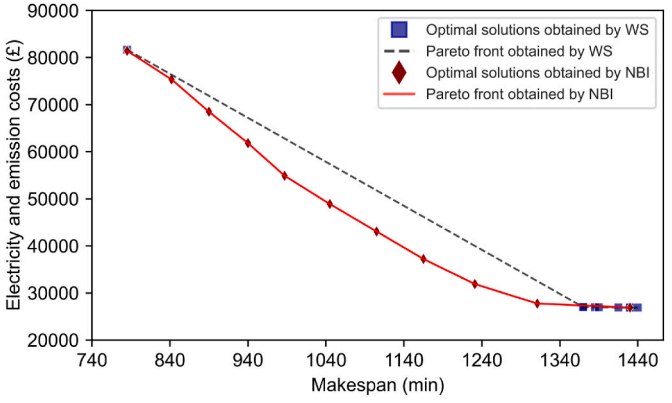

Fig. 11. Comparison of solution distribution obtained by the WS and NBI method (11 optimal solutions).

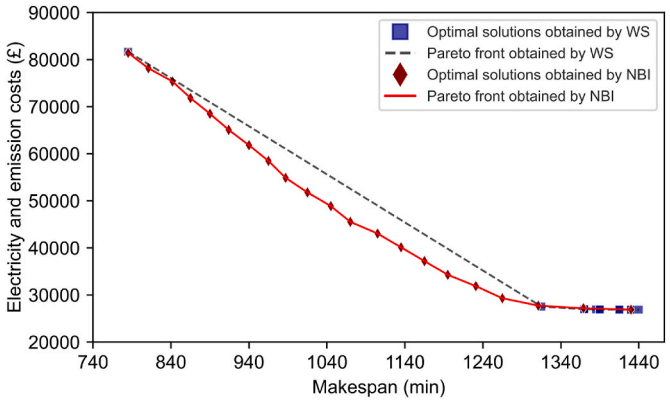

Fig. 12. Comparison of solution distribution obtained by the WS and NBI method (21 optimal solutions).

based strategy for providing representative optimal solutions, enabling the plant operator to adjust to changing order urgencies by choosing the most suitable schedules from the provided optimal solutions set when navigating variability in PTR for enhancing the adaptability and responsiveness of model.

5.2.3. Sensitivity analysis of the carbon tax

Since the carbon tax affects the value of the cost objective, it is necessary to conduct sensitivity analyses of the carbon tax. We design two cases where Min EL-EM refers to the minimisation of electricity and emission costs, while Min EL refers to the minimisation of electricity cost only. We separately discuss the impact of the carbon tax on the electricity and emission costs and the indirect emissions.

Fig. 13 displays a comparison of electricity and emission costs of two cases. From the results, we can observe that Min EL-EM save more on total costs compared to Min EL as the carbon tax increases. Fig. 14 shows the sensitivity of the indirect emission to carbon tax for two cases, where Min EL is insensitive to the increase of carbon tax, with a constant indirect emissions of about 77 tCO2e. On the contrary, in Min EL-EM, the production scheduling is responsive to carbon taxes, resulting in a decreasing pattern in indirect emissions as the carbon tax increases. The most significant drop appears when the carbon tax moves from 0 to 60 in the unit of £/tCO2e, while the indirect emissions remain almost constant as the carbon tax increases from 60 to 160.

We can obtain the following insights: 1) with a given electricity price, the increase in carbon tax will motivate the steelmaking plant to consider emissions in their scheduling; 2) as the electricity price increases, the carbon tax needs to correspondingly increase to keep an

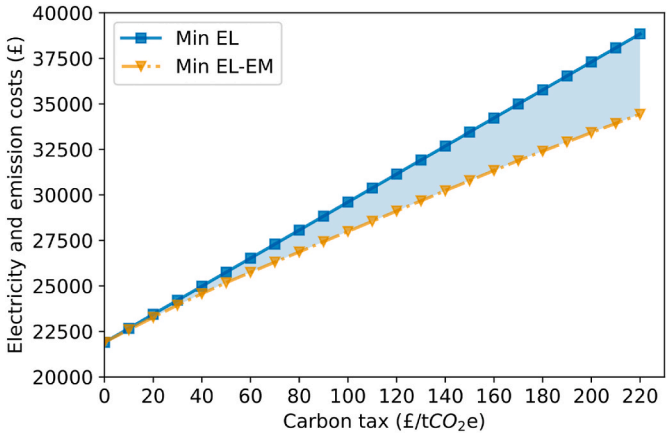

Fig. 13. Electricity and emission cost sensitivity of the carbon tax when make-span is 1430 min.

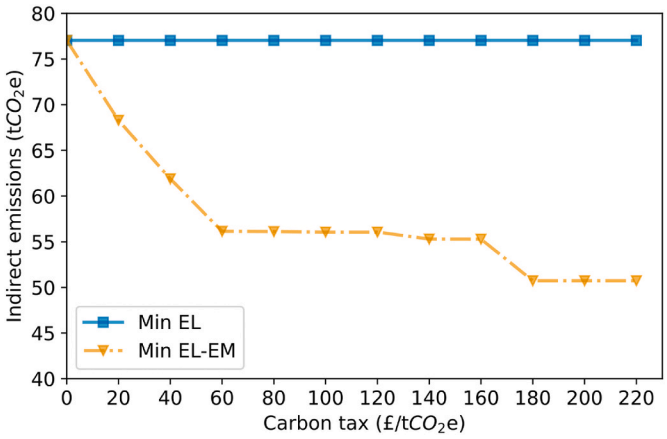

Fig. 14. Indirect emission sensitivity of the carbon tax when make-span is 1430 min.

economic impact on the production scheduling of the plant.

6. Conclusion and future research

This paper set out to develop a multi-objective scheduling model for a steelmaking plant integrated with RES and ESS, considering the variability in the PTR of steel production orders. Firstly, the MO-MILP model is established based on the extended RTN formulations. Then, the what-if-analysis-based strategy coupled with the NBI method is proposed to generate a series of evenly distributed Pareto optimal points tailored to different make-span scenarios. Finally, the BESS is integrated to further improve the time granularity of the steelmaking plant's flexibility.

The results of the numerical simulations indicate that our proposed method can provide a series of evenly distributed Pareto optimal points tailored to different make-span scenarios. Meanwhile, the proposed scheduling model can reduce the electricity and emission costs by 68.5%, reduce indirect emissions by 83.5%, and increase the on-site RES self-consumption rate by 12.1%. Furthermore, the integration of BESS brings a downward shift of the Pareto front, indicating the improvement of time granularity of the steelmaking plant's flexibility. With the improved responsiveness, a further 4.3% decrement in electricity and emission costs is achieved. Considering continuous investment cost reduction and the prevalence of RES and ESS, more and more steelmaking plants will install these facilities. This paper sheds light on the cooperation between the steelmaking process and clean energy sources, implying its great relevance to the development of a cleaner steel industry in the future.

Prospective improvements of our work include: first, the proposed method relies on the accurate prediction of some parameters such as RES generation. Although the existence of prediction errors might compromise the performance of the obtained solutions, they can be mitigated by developing rescheduling strategies. Thus, we will focus on developing an intra-day rescheduling strategy for the steelmaking plant considering the realisation of the above-mentioned uncertain factors. Furthermore, some parameters are selected based on experience, such as the ESS capacity and the amount of Pareto solutions. Although the effectiveness of the proposed method does not deteriorate, an optimal parameter selection method is helpful to guide its real-world deployment, which will be another future work.

CRediT authorship contribution statement

Pengfei Su: Conceptualization, Investigation, Methodology, Software, Visualization, Writing – original draft. **Yue Zhou:** Project administration, Conceptualization, Supervision, Resources, Writing – review & editing. **Jianzhong Wu:** Project administration,

Conceptualization, Supervision, Writing – review & editing.

Declaration of competing interest

The authors declare that they have no known competing financial interests or personal relationships that could have appeared to influence the work reported in this paper.

Data availability

Information about the data used in the case study of this paper, including how to access them, can be found in the Cardiff University data catalogue at http://doi.org/10.17035/d.2023.0291344811.

Acknowledgement

We thank Hongyi Li (University of Macau) for assistance throughout revision, and Dr. Wei Gan (Cardiff University) for useful discussions. This work was supported by the China Scholarship Council, China and EPSRC, United Kingdom through the projects EP/T021969/1 (MC2), EP/W028573/1 (Digital Twin with Data-Driven Predictive Control: Unlocking Flexibility of Industrial Plants for Supporting a Net Zero Electricity System), and SFSC2-203 (Smart and Flexible Operation of Steelmaking Plants in a Net-Zero Electricity System – A Digital Twin Approach) as a feasibility study funded by EP/S018107/1 (SUSTAIN Manufacturing Hub).

References

Ashok, S., 2006. Peak-load management in steel plants. Appl. Energy 83, 413–424. https://doi.org/10.1016/j.apenergy.2005.05.002.

Castro, P., Ave, G.D., Harjunkoski, I., Grossmann, I., 2019. Demand side management of a steel plant incorporating the maintenance of EAFs with alternative operating modes. In: 2019 AIChE Annual Meeting. AIChE. Presented at the.

Castro, P.M., Dalle Ave, G., Engell, S., Grossmann, I.E., Harjunkoski, I., 2020. Industrial demand side management of a steel plant considering alternative power modes and electrode replacement. Ind. Eng. Chem. Res. 59, 13642–13656. https://doi.org/10.1021/acs.iecr.0c01714.

Castro, P.M., Harjunkoski, I., Grossmann, I.E., 2009. New continuous-time scheduling formulation for continuous plants under variable electricity cost. Ind. Eng. Chem. Res. 48, 6701–6714. https://doi.org/10.1021/ie900073k.

Castro, P.M., Sun, L., Harjunkoski, I., 2013. Resource–task network formulations for industrial demand side management of a steel plant. Ind. Eng. Chem. Res. 52, 13046–13058. https://doi.org/10.1021/ie401044q.

Chen, W., Wang, J., Yu, G., 2022. Energy-efficient scheduling for an energy-intensive industry under punitive electricity price. J. Clean. Prod. 373, 133851 https://doi.org/10.1016/j.jclepro.2022.133851.

Das, I., Dennis, J.E., 1998. Normal-boundary intersection: a new method for generating the Pareto surface in nonlinear multicriteria optimization problems. SIAM J. Optim. 8, 631–657. https://doi.org/10.1137/S1052623496307510.

Hadera, H., Harjunkoski, I., Sand, G., Grossmann, I.E., Engell, S., 2015. Optimization of steel production scheduling with complex time-sensitive electricity cost. Comput. Chem. Eng. 76, 117–136. https://doi.org/10.1016/j.compchemeng.2015.02.004.

Harjunkoski, I., Grossmann, I.E., 2001. A decomposition approach for the scheduling of a steel plant production. Comput. Chem. Eng. 25, 1647–1660. https://doi.org/10.1016/S0098-1354(01)00729-3.

Harjunkoski, I., Maravelias, C.T., Bongers, P., Castro, P.M., Engell, S., Grossmann, I.E., Hooker, J., Méndez, C., Sand, G., Wassick, J., 2014. Scope for industrial applications of production scheduling models and solution methods. Comput. Chem. Eng. 62, 161–193. https://doi.org/10.1016/j.compchemeng.2013.12.001.

Harjunkoski, I., Sand, G., 2008. Flexible and configurable MILP-models for meltshop scheduling optimization. In: Braunschweig, B., Joulia, X. (Eds.), Computer Aided Chemical Engineering, 18 European Symposium on Computer Aided Process Engineering. Elsevier, pp. 677–682. https://doi.org/10.1016/S1570-7946(08)80118-6.

IEA, 2020. Iron and Steel Technology Roadmap. IEA, Paris.

Iglesias-Escudero, M., Villanueva-Balsera, J., Ortega-Fernandez, F., Rodriguez-Montequín, V., 2019. Planning and scheduling with uncertainty in the steel sector: a review. Appl. Sci. 9, 2692. https://doi.org/10.3390/app9132692.

International Society of Automation (ISA), 2020. Enterprise-control System Integration – Part 8: Information Exchange Profiles.

Ju, C., Wang, P., Goel, L., Xu, Y., 2018. A two-layer energy management system for microgrids with hybrid energy storage considering degradation costs. IEEE Trans. Smart Grid 9, 6047–6057. https://doi.org/10.1109/TSG.2017.2703126.

Li, H., Hui, H., Zhang, H., 2023. Blockchain-assisted virtual power plant framework for providing operating reserve with various distributed energy resources. iEnergy 2, 133–142. https://doi.org/10.23919/IEN.2023.0013.

National Grid, E.S.O., 2023a. ESO data portal: embedded solar and wind forecast - dataset. National Grid Electricity System Operator [WWW Document]. URL. https://data.nationalgrideso.com/generation/embedded-wind-and-solar-forecasts/r/embedded_solar_and_wind_forecast. (Accessed 4 October 2023).

National Grid, E.S.O., 2023b. Carbon intensity API [WWW Document]. URL. https://carbonintensity.org.uk/. (Accessed 13 May 2023).

NORD, P.O.O.L., 2023. GB half hourly day-ahead auction prices [WWW Document]. URL. https://www.nordpoolgroup.com/en/Market-data1/GB/half-hourly-prices/gb/half-hour/. (Accessed 4 July 2023).

Pantelides, C.C., 1994. Unified frameworks for optimal process planning and scheduling. In: Proceedings on the Second Conference on Foundations of Computer Aided Operations, pp. 253–274.

Pfenninger, S., Staffell, I., 2016. Long-term patterns of European PV output using 30 years of validated hourly reanalysis and satellite data. Energy 114, 1251–1265. https://doi.org/10.1016/j.energy.2016.08.060.

Ramin, D., Spinelli, S., Brusaferri, A., 2018. Demand-side management via optimal production scheduling in power-intensive industries: the case of metal casting process. Appl. Energy 225, 622–636. https://doi.org/10.1016/j.apenergy.2018.03.084.

Roman, C., Rosehart, W., 2006. Evenly distributed Pareto points in multi-objective optimal power flow. IEEE Trans. Power Syst. 21, 1011–1012. https://doi.org/10.1109/TPWRS.2006.873010.

Shukla, P.K., Deb, K., 2007. On finding multiple Pareto-optimal solutions using classical and evolutionary generating methods. Eur. J. Oper. Res. 181, 1630–1652. https://doi.org/10.1016/j.ejor.2006.08.002.

Sun, W., Wang, Q., Zhou, Y., Wu, J., 2020. Material and energy flows of the iron and steel industry: status quo, challenges and perspectives. Appl. Energy 268, 114946. https://doi.org/10.1016/j.apenergy.2020.114946.

Trevino-Martinez, S., Sawhney, R., Shylo, O., 2022. Energy-carbon footprint optimization in sequence-dependent production scheduling. Appl. Energy 315, 118949. https://doi.org/10.1016/j.apenergy.2022.118949.

Wang, J., Wang, Q., Sun, W., 2023a. Optimal power system flexibility-based scheduling in iron and steel production: a case of steelmaking–refining–continuous casting process. J. Clean. Prod. 137619 https://doi.org/10.1016/j.jclepro.2023.137619.

Wang, J., Wang, Q., Sun, W., 2023b. Quantifying flexibility provisions of the ladle furnace refining process as cuttable loads in the iron and steel industry. Appl. Energy 342, 121178. https://doi.org/10.1016/j.apenergy.2023.121178.

Xiong, H., Shi, S., Ren, D., Hu, J., 2022. A survey of job shop scheduling problem: the types and models. Comput. Oper. Res. 142, 105731 https://doi.org/10.1016/j.cor.2022.105731.

Xu, X., Abeysekera, M., Gutschi, C., Qadrdan, M., Rittmannsberger, K., Markus, W., Wu, J., Jenkins, N., 2020. Quantifying flexibility of industrial steam systems for ancillary services: a case study of an integrated pulp and paper mill. IET Energy Systems Integration 2, 124–132. https://doi.org/10.1049/iet-esi.2019.0082.

Xu, X., Sun, W., Abeysekera, M., Qadrdan, M., 2021. Quantifying the flexibility from industrial steam systems for supporting the power grid. IEEE Trans. Power Syst. 36, 313–322. https://doi.org/10.1109/TPWRS.2020.3007720.

Zhang, H., Zhao, F., Fang, K., Sutherland, J.W., 2014. Energy-conscious flow shop scheduling under time-of-use electricity tariffs. CIRP Annals 63, 37–40. https://doi.org/10.1016/j.cirp.2014.03.011.

Zhang, X., Hug, G., Harjunkoski, I., 2017. Cost-effective scheduling of steel plants with flexible EAFs. IEEE Trans. Smart Grid 8, 239–249. https://doi.org/10.1109/TSG.2016.2575000.

Zhang, X., Hug, G., Kolter, J.Z., Harjunkoski, I., 2018. Demand response of ancillary service from industrial loads coordinated with energy storage. IEEE Trans. Power Syst. 33, 951–961. https://doi.org/10.1109/TPWRS.2017.2704524.